JOURNAL OF COMPUTATIONAL PHYSICS 82, 193–217 (1989)

The Evolution and Discharge of Electric Fields within a Thunderstorm*

WILLIAM W. HAGER,† JOHN S. NISBET, AND JOHN R. KASHA

Communications and Space Sciences Laboratory, Department of Electrical Engineering, The Pennsylvania State University, University Park, Pennsylvania 16802

Received February 5, 1988; revised July 19, 1988

A 3-dimensional electrical model for a thunderstorm is developed and finite difference approximations to the model are analyzed. If the spatial derivatives are approximated by a method akin to the box scheme and if the temporal derivative is approximated by either a backward difference or the Crank–Nicholson scheme, we show that the resulting discretization is unconditionally stable. The forward difference approximation to the time derivative is stable when the time step is sufficiently small relative to the ratio between the permittivity and the conductivity. Max-norm error estimates for the discrete approximations are established. To handle the propagation of lightning, special numerical techniques are devised based on the Inverse Matrix Modification Formula and Çholesky updates. Numerical comparisons between the model and theoretical results of Wilson and Holzer-Saxon are presented. We also apply our model to a storm observed at the Kennedy Space Center on July 11, 1978.

1. INTRODUCTION

In this paper, we develop a 3-dimensional model for the evolution of the electric field in a thunderstorm. The output of the model is the electric field as a function of time while the inputs are currents generated by the flow of charged particles within the thundercloud. In earlier work, Nisbet [16] developed a cylindrically symmetric model and he solved the discrete equations using an electronic circuit analysis program called ECAP. Later Forbes *et al.* [5] showed that the horizontal structure of a thundercloud is of fundamental importance to the electrification, and to make realistic comparisons between data and theory, a 3-dimensional unsymmetric model was needed. On the other hand, the circuit analysis approach used by

* This research was supported by the National Aeronautics and Space Administration under Grant NGL 39-009-003, by the National Science Foundation under Grants ATM 8311993 and DMS 8520926, and by the Air Force Office of Scientific Research under Grant AFOSR-ISSA-860091. The numerical computations were performed at the John von Neumann Computer Center under grants NAC-806 and NAC-824.

† This author is also a member of the Mathematics Department, University of Florida, Gainesville, FL 32611.

0021-9991/89 $3.00

Nisbet in [16] is impractical for 3-dimensional unsymmetric problems since the computational effort and the storage associated with each time step are very large. We now develop a thunderstorm model that is more tractable numerically.

From Maxwell's equations, we obtain a relation between the potential field and current density. The spatial derivatives in this equation are approximated by a method akin to the box scheme (see [24]); that is, the domain is decomposed into boxes, the partial differential equation is integrated over each box, the divergence theorem is applied, and spatial derivatives in the resulting boundary integrals are approximated by central differences. A 1-parameter family of time discretizations is studied. This family includes forward difference, backward difference, and Crank–Nicholson approximations. Both the backward difference and the Crank–Nicholson approximations are unconditionally stable while the forward difference is stable when the time step is sufficiently small relative to the ratio between the permittivity and the conductivity. For a stable scheme, a max-norm error estimate of the form $O(\Delta t^m) + O(h^2)$ is established where Δt and h are the temporal and the spatial discretization parameters and $m = 2$ for the Crank–Nicholson scheme while $m = 1$ otherwise.

When the electric field reaches the breakdown threshold, the cloud discharges since the conductivity in the breakdown region is very large. To compute the impact of this electrical discharge on the potential field, we observe that changing the conductivity in a region is equivalent to adding a small rank correction to the coefficient matrix associated with the discrete equations. As the conductivity tends to infinity, the adjustment in the potential throughout the cloud caused by this correction term can be computed explicitly using the Inverse Matrix Modification Formula (see [8]). Essentially the electrical discharge readjusts the potential field throughout the domain so that in the breakdown region, the potential is a constant. In other words, the discharge process equilibrates the potential throughout the breakdown region. An efficient numerical implementation of this method to handle the electrical discharge is presented.

The paper concludes with some numerical experiments. In the first two experiments, we solve problems with known solutions: In [26] Wilson computes the electric field generated by a current impulse, and in [12] Holzer and Saxon compute the electric field produced by a step function generator. Comparing the numerical solution to the known solution, we are able to determine the error in the numerical approximation. In these first two experiments, the electric field does not break down and we essentially measure the spatial error in our discrete approximation. In the third experiment, we present some preliminary results for a simulation of a thunderstorm observed at the Kennedy Space Center on July 11, 1978. In this simulation, the electric field repeatedly reaches the breakdown threshold. A more extensive study of this storm as well as other numerical comparisons will be reported in a separate paper.

In related work [1], Browning, Tzur, and Roble study the well-posedness of the partial differential equation governing the evolution of the electric potential. In addition they obtain some special solutions to this equation, giving incite into the

relative time scales in a thunderstorm. A different way to analyze well-posedness appears in Section 2 of our paper where we show that the potential field can be expressed in terms of the solution to an abstract first-order differential equation.

2. Formulation of the Equations

By Maxwell's equations, the curl of the magnetic field strength $\mathbf{H}$ is given by

$$\nabla \times \mathbf{H} = \varepsilon \frac{\partial \mathbf{E}}{\partial t} + \sigma \mathbf{E} + \mathbf{J}, \tag{1}$$

where ε is the permittivity, σ is the conductivity, $\mathbf{E}$ is the electric field, $\mathbf{J}$ is the current density associated with charged particles circulating in the cloud, $\sigma\mathbf{E}$ is the conduction current density, and $\varepsilon(\partial\mathbf{E}/\partial t)$ is the displacement current density. In the atmosphere, σ typically depends on the altitude. Moreover, σ depends on the electric field in the following sense: Whenever the electric field reaches some breakdown threshold, σ increases by many orders of magnitude. As indicated in Section 1, we will compute $\mathbf{E}$ assuming that $\mathbf{J}$ is known. Methods for estimating $\mathbf{J}$ are discussed in Section 7.

To eliminate $\mathbf{H}$ from Eq. (1), we take the divergence to obtain:

$$\varepsilon \nabla \cdot \frac{\partial \mathbf{E}}{\partial t} + \nabla \cdot \sigma \mathbf{E} + \nabla \cdot \mathbf{J} = 0.$$

In our model, it is assumed that the time derivative of the magnetic field is zero. Hence, the curl of the electric field is zero, $\nabla \times \mathbf{E} = \mathbf{0}$, and $\mathbf{E}$ is the gradient of a potential ϕ. Substituting $\mathbf{E} = \nabla\phi$ gives

$$\varepsilon \frac{\partial \nabla^2 \phi}{\partial t} + \sigma \nabla^2 \phi + \nabla\sigma \cdot \nabla\phi + \nabla \cdot \mathbf{J} = 0, \tag{2}$$

where ∇^2 denotes the Laplacian operator defined by $\nabla^2 = \nabla \cdot \nabla$. Letting ψ denote the Laplacian of ϕ, we have

$$\varepsilon \frac{\partial \psi}{\partial t} + \sigma\psi + \nabla\sigma \cdot \nabla\phi + \nabla \cdot \mathbf{J} = 0, \qquad \psi = \nabla^2\phi. \tag{3}$$

If σ is independent of position, then $\nabla\sigma = 0$ and Eq. (3) can be integrated to obtain ψ (or equivalently to obtain $\nabla^2\phi$) at any time. Knowing ψ and the boundary values of ϕ, we can solve the Poisson equation $\nabla^2\phi = \psi$ for ϕ. On the other hand, for the atmosphere, σ depends on position and the $\nabla\sigma \cdot \nabla\phi$ term in (3) cannot be ignored.

The natural domain for a thunderstorm is the half-space in three dimensions defined by $z \geqslant 0$. Treating the earth as a perfect conductor, the natural boundary condition is the Dirichlet condition $\phi(x, y, 0) = 0$; that is, the potential vanishes on

the surface of the earth. With these boundary conditions, the solution ϕ to $\nabla^2\phi = \psi$ can be expressed in terms of the Green's function G,

$$\phi(\mathbf{r}) = \int_s G(\mathbf{r}, \mathbf{s})\psi(\mathbf{s}), \tag{4}$$

where

$$4\pi G(\mathbf{r}, \mathbf{s}) = \frac{1}{|\mathbf{r}-\mathbf{s}|} - \frac{1}{|\boldsymbol{\rho}-\mathbf{s}|},$$

and $\boldsymbol{\rho}$ is the reflection of $\mathbf{r}$ across the plane $z = 0$. Combining (3) and (4) yields

$$\varepsilon\frac{\partial\psi}{\partial t} + \sigma\psi + \nabla\sigma \cdot \int_s \nabla G(\mathbf{r}, \mathbf{s})\psi(\mathbf{s}) + \nabla \cdot \mathbf{J} = 0. \tag{5}$$

Abstractly, Eq. (5) has the form

$$\varepsilon\frac{\partial\psi}{\partial t} + L\psi + f = 0, \tag{6}$$

where L is a linear operator and $f = \nabla \cdot \mathbf{J}$. Thus one way to compute the electric field is to integrate Eq. (6) from some starting condition to obtain ψ, compute ϕ by evaluating the integral (4), and differentiate ϕ to obtain $\mathbf{E} = \nabla\phi$. It follows from (6) that ψ has one more time derivative than f and if f varies smoothly in space and time, then ϕ varies smoothly in space and time. This formulation of the equations for the electric field provides some indication of the regularity of the solution to (2).

3. Discretized Equations

We will describe the discretization process for a uniform mesh in a rectangular coordinate system. However, in practice it is better to use a cylindrical coordinate system; since the electric field changes rapidly near a current generator and slowly far from a current generator, a fine mesh should be employed near a current generator and a coarse mesh should be used far from the generator—a cylindrical coordinate system centered at the generator is well suited for this type of mesh. If there are several current generators, then a cylindrical coordinate system can be placed at each generator and the total electric field can be computed using a superposition technique. For reference, Appendix 1 presents the discretization based on a cylindrical coordinate system.

Our first approximation is to replace the half-space by a large box. For a thundercloud, the dimensions of the box are on the order of $100 \times 100 \times 100$ kilometers since the currents in a thundercloud flow in the earth-ionosphere circuit. There is some flexibility in the choice of boundary conditions for ϕ since the electric field as

well as the potential approaches zero as we move away from the center of the thundercloud. In our numerical experiments, either Neumann or Dirichlet boundary conditions were employed on the sides and on the top of the box; that is, either ϕ or its normal derivative vanishes on the sides and the top of the box. Treating the earth as a perfect conductor, ϕ vanishes on the bottom of the box. Next we partition the box into small cubes with sides of length h. The center of a typical cube is denoted (x_i, y_j, z_k) and the centers of the neighboring cubes are $(x_{i\pm1}, y_{j\pm1}, z_{k\pm1})$. Although the input for Eq. (2) is the current density, it is often easier to estimate currents. To convert from current density to current, we integrate Eq. (2) over the cube S_{ijk} containing the point (x_i, y_j, z_k) and we apply the divergence theorem to obtain

$$\int_{\partial S_{ijk}} \varepsilon \frac{\partial \nabla\phi}{\partial t} \cdot \mathbf{dS} + \int_{\partial S_{ijk}} \sigma \nabla\phi \cdot \mathbf{dS} + I = 0, \tag{7}$$

where I is the net current leaving S_{ijk} and ∂S_{ijk} is the boundary of S_{ijk}.

We discretize the time derivative in (7) using Euler's finite difference approximation. Let a superscript n denote the time level t_n, let Δt denote the time step $t_{n+1} - t_n$, and let μ denote an arbitrary parameter between 0 and 1. The following family of time discretizations for (7) is considered:

$$\varepsilon \int_{\partial S_{ijk}} \frac{\nabla\phi^{n+1} - \nabla\phi^n}{\Delta t} \cdot \mathbf{dS} + \int_{\partial S_{ijk}} \sigma^n [\mu \nabla\phi^{n+1} + (1-\mu)\nabla\phi^n] \cdot \mathbf{dS} + I^{n+1/2} = 0. \tag{8}$$

Here the current term is evaluated at time $\frac{1}{2}(t_{n+1} + t_n)$, which is denoted time level $n + \frac{1}{2}$. By analogy with the terminology used for the heat equation, $\mu = 1$ is the backward Euler scheme, $\mu = 0$ is the forward Euler scheme, and $\mu = \frac{1}{2}$ is the Crank–Nicholson scheme. Unlike the heat equation, the discretization (8) is implicit for all values of μ since the time derivative term in (7) contains the gradient of the potential.

The spatial part of (8) can also be discretized using Euler's finite difference approximation. Let ϕ_{ijk} denote the discrete approximation to ϕ at the point (x_i, y_j, z_k). The derivative $\partial\phi/\partial x$ at the midpoint of the line segment connecting (x_i, y_j, z_k) to (x_{i+1}, y_j, z_k) has an approximation which we denote by $\partial_1^+ \phi_{ijk}$:

$$\partial_1^+ \phi_{ijk} = \frac{\phi_{i+1,j,k} - \phi_{ijk}}{h}.$$

In similar manner, we define approximations $\partial_2^+ \phi_{ijk}$ and $\partial_3^+ \phi_{ijk}$ to the partial derivatives $\partial\phi/\partial y$ and $\partial\phi/\partial z$:

$$\partial_2^+ \phi_{ijk} = \frac{\phi_{ij+1,k} - \phi_{ijk}}{h} \quad \text{and} \quad \partial_3^+ \phi_{ijk} = \frac{\phi_{ij,k+1} - \phi_{ijk}}{h}, \quad \text{respectively.}$$

We also define the shifted approximations $\partial_1^- \phi_{ijk} = \partial_1^+ \phi_{i-1,j,k}$, $\partial_2^- \phi_{ijk} = \partial_2^+ \phi_{i,j-1,k}$, $\partial_3^- \phi_{ijk} = \partial_3^+ \phi_{i,j,k-1}$. Integrating around the boundary of S_{ijk}, we have

$$\int_{\partial S_{ijk}} \nabla\phi \cdot \mathbf{dS} \approx h^3 \left(h^{-1} \sum_{l=1}^{3} [\partial_l^+ - \partial_l^-] \right) \phi_{ijk}. \tag{9}$$

Note that the expression in parentheses is the standard 7-point approximation to the Laplacian operator.

For the conductivity term in (8), we must take into acount the variation of the conductivity with position. In the atmosphere, σ varies with altitude. Assuming the σ is independent of x and y, a similar approximation to (9) can be applied to the sides of the cube parallel to the xy-plane. For sides of the cube parallel to the xz-plane and the yz-plane, we must introduce an average conductivity. To help motivate this average, let us examine some quadrature rules for the integral of a product. The standard trapezoidal approximation to the integral of a product is

$$\int_a^b f(z)\, g(z)\, dz \approx (b-a) f(c)\, g(c),$$

where c is the midpoint of the interval $[a, b]$. The error in the trapezoidal rule is given by

$$\int_a^b f(z)\, g(z)\, dz - (b-a)\, f(c)\, g(c) = \frac{(b-a)^3}{24} \frac{d^2[f(z)\, g(z)]}{dz^2}\bigg|_{z=\zeta}, \tag{10}$$

where ζ lies between a and b. However, when f is a slowing varying function and g is a rapidly varying function, a better approximation to the integral of a product is

$$\int_\alpha^b f(z)\, g(z)\, dz \approx f(c) \int_a^b g(z)\, dz. \tag{11}$$

With this alternative approximation, one less derivative of g appears in the error expression and the error is less sensitive to the derivative of g. For example, merely assuming that g and f' are essentially bounded, we have the estimate

$$\left| \int_a^b f(z)\, g(z)\, dz - f(c) \int_a^b g(z)\, dz \right| \leqslant \frac{(b-a)^2}{4} \|g\|\, \|f'\|,$$

where $\|\cdot\|$ denotes the essential supremum. And if both f'' and g' are essentially bounded, then the error is bounded by an expression involving the bounds on these derivatives times $(b-a)^3$. In contrast, by (10) the corresponding error bound for the trapezoidal rule involves the second derivative of g.

For the atmosphere, σ varies almost exponentially with altitude. The exponential function that agrees with g at $z=a$ and at $z=b$ is

$$g(a)e^{\alpha(z-a)}, \qquad \text{where} \quad \alpha=\frac{\log_e[g(b)/g(a)]}{b-a}.$$

Integrating this exponential over z between a and b and combining with (11) gives us the approximation

$$\int_a^b f(z)\,g(z)\,dz \approx (b-a)\,f(c)\,\frac{g(b)-g(a)}{\log_e g(b)-\log_e g(a)}.$$

Now return to the conductivity term in (8). Letting ζ_k denote the average of z_k and z_{k-1}:

$$\zeta_k=\frac{z_k+z_{k-1}}{2},$$

we define an average conductivity σ_k by the rule

$$\sigma_k=\frac{\sigma(\zeta_{k+1})-\sigma(\zeta_k)}{\log_e \sigma(\zeta_{k+1})-\log_e \sigma(\zeta_k)}. \tag{12}$$

Then we have the following approximation corresponding to the conductivity term in (8):

$$\int_{\partial S_{ijk}} \sigma\,\nabla\phi\cdot\mathbf{dS} \approx h^2\left[\sigma_k \sum_{l=1}^{2}(\partial_l^+ - \partial_l^-)+\sigma(\zeta_{k+1})\partial_3^+ - \sigma(\zeta_k)\partial_3^-\right]\phi_{ijk}. \tag{13}$$

4. Stability and Convergence

The temporal discretization (8) and the spatial discretizations (9) and (13) combine to yield a matrix-vector relation of the form

$$\mathbf{A}[\mathbf{\Phi}^{n+1}-\mathbf{\Phi}^n]+\Delta t\,\mathbf{B}[\mu\mathbf{\Phi}^{n+1}+(1-\mu)\mathbf{\Phi}^n]=\Delta t\,\mathbf{I}^n, \tag{14}$$

where $\mathbf{\Phi}$ denotes the vector with components ϕ_{ijk} and $\mathbf{I}^n$ corresponds to the current term of (8) evaluated at time level $n+\frac{1}{2}$. The matrices $\mathbf{A}$ and $\mathbf{B}$ are symmetric and by the corollary on page 23 of Varga's book [24], we know that they are also positive definite. Since the sum of positive definite matrices is positive definite, $\mathbf{A}+\Delta t\,\mu\mathbf{B}$ is positive definite and we can solve for $\mathbf{\Phi}^n$ in (14):

$$\mathbf{\Phi}^{n+1}=\mathbf{C}^{-1}\mathbf{D}\mathbf{\Phi}^n+\Delta t\,\mathbf{C}^{-1}\mathbf{I}^n, \tag{15}$$

where $\mathbf{C}=\mathbf{A}+\Delta t\,\mu\mathbf{B}$ and $\mathbf{D}=\mathbf{A}-\Delta t(1-\mu)\mathbf{B}$. This finite difference relation is con-

sidered stable if the amplification matrix $\mathbf{C}^{-1}\mathbf{D}$ has spectral radius less than one. Since $\mathbf{C}^{-1}\mathbf{D}$ is similar to the symmetric matrix $\mathbf{C}^{-1/2}\mathbf{D}\mathbf{C}^{-1/2}$, it follows that the eigenpairs of the matrix $\mathbf{C}^{-1}\mathbf{D}$ are real. Let $(\lambda, \mathbf{x})$ denote an eigenpair for $\mathbf{C}^{-1}\mathbf{D}$. Multiplying the relation $\mathbf{C}^{-1}\mathbf{D}\mathbf{x} = \lambda\mathbf{x}$ by $\mathbf{x}^{\mathrm{T}}\mathbf{C}$ and solving for λ, we have

$$\lambda = \frac{\mathbf{x}^{\mathrm{T}}\mathbf{D}\mathbf{x}}{\mathbf{x}^{\mathrm{T}}\mathbf{C}\mathbf{x}} = \frac{\mathbf{x}^{\mathrm{T}}(\mathbf{A} - \Delta t(1-\mu)\,\mathbf{B})\mathbf{x}}{\mathbf{x}^{\mathrm{T}}(\mathbf{A} + \Delta t\,\mu\mathbf{B})\mathbf{x}} = 1 - \frac{\Delta t\,\mathbf{x}^{\mathrm{T}}\mathbf{B}\mathbf{x}}{\mathbf{x}^{\mathrm{T}}(\mathbf{A} + \Delta t\,\mu\mathbf{B})\mathbf{x}}. \tag{16}$$

Since $\mathbf{A}$ and $\mathbf{B}$ are positive definite, $\lambda < 1$ for every $\mu \geqslant 0$. By the second equality in (16), it follows that $\lambda > -1$ when μ is between $\frac{1}{2}$ and 1. Hence, the scheme (14) is unconditionally stable for μ between $\frac{1}{2}$ and 1. For μ in the range $0 \leqslant \mu < \frac{1}{2}$, the scheme is stable for Δt sufficiently small.

Suppose that σ is a constant independent of position. Then the expression (16) reduces to

$$\lambda = \frac{\varepsilon - \sigma\,\Delta t(1-\mu)}{\varepsilon + \sigma\,\Delta t\,\mu}.$$

Thus $\lambda \geqslant -1$ for $\mu < \frac{1}{2}$ if and only if

$$\Delta t \leqslant \frac{2\varepsilon}{\sigma(1-2\mu)}. \tag{17}$$

The discretized version of (7) is similar to the discretized heat equation in that (14) is unconditionally stable for $\frac{1}{2} \leqslant \mu \leqslant 1$ while conditionally stable for $0 \leqslant \mu < \frac{1}{2}$. However, with the heat equation, the stability condition for $\mu < \frac{1}{2}$ involves the spatial parameter h while (17) is independent of h.

Now suppose that σ varies continuously with position and $0 \leqslant \mu < \frac{1}{2}$. Again, by (16) $\lambda < 1$ while $\lambda \geqslant -1$ if

$$\Delta t \leqslant \frac{2}{1-2\mu}\,\frac{\mathbf{x}^{\mathrm{T}}\mathbf{A}\mathbf{x}}{\mathbf{x}^{\mathrm{T}}\mathbf{B}\mathbf{x}}$$

for every eigenvector $\mathbf{x}$ of $\mathbf{C}^{-1}\mathbf{D}$. Hence, $\lambda \geqslant -1$ if

$$\Delta t \leqslant \frac{2}{1-2\mu}\,\max_{\mathbf{x}\neq\mathbf{0}}\,\frac{\mathbf{x}^{\mathrm{T}}\mathbf{A}\mathbf{x}}{\mathbf{x}^{\mathrm{T}}\mathbf{B}\mathbf{x}}.$$

We will show that

$$\operatorname*{maximum}_{\mathbf{x}\neq\mathbf{0}}\,\frac{\mathbf{x}^{\mathrm{T}}\mathbf{A}\mathbf{x}}{\mathbf{x}^{\mathrm{T}}\mathbf{B}\mathbf{x}} \leqslant \frac{\varepsilon}{\text{maximum } \sigma}, \tag{18}$$

where the phrase "maximum σ" means the maximum value for the conductivity

over the domain. It follows that the finite difference equation (15) is stable for μ between 0 and $\frac{1}{2}$ if

$$\Delta t \leqslant \frac{2}{1-2\mu} \frac{\varepsilon}{\text{maximum } \sigma}.$$

To establish (18), we first note that if g is continuous, there exists a point $\bar{z}$ between a and b such that

$$\int_a^b g(z)\, dz = (b-a)\, g(\bar{z}).$$

If g is a monotone function (like the exponential function), then $g(\bar{z})$ lies between $g(a)$ and $g(b)$. Since the exponential approximation to σ described in Section 3 agrees with σ at $z=\zeta_k$ and $z=\zeta_{k+1}$, the $g(\bar{z})$ corresponding to the interval $[\zeta_k, \zeta_{k+1}]$ lies between $\sigma(\zeta_k)$ and $\sigma(\zeta_{k+1})$. It follows that $\mathbf{x}^{\mathrm{T}}\mathbf{B}\mathbf{x}$ can be written in the form

$$\mathbf{x}^{\mathrm{T}}\mathbf{B}\mathbf{x} = h^2 \sum_{i,j,k,l} \sigma_{ijkl} [\partial_l^+ x_{ijk}]^2,$$

where σ_{ijkl} is either the value of the conductivity at some point or σ_{ijkl} lies between two values of the conductivity. Clearly, replacing any of the parameters σ_{ijkl} by something larger increases $\mathbf{x}^{\mathrm{T}}\mathbf{B}\mathbf{x}$. Replacing σ_{ijkl} by the maximum of σ over the domain yields (18).

The error in the discrete approximation $\mathbf{\Phi}^n$ is related to the truncation error that results from inserting the continuous solution $\phi(x_i, y_j, z_k, t_n)$ into the discrete equation (14). Let $\mathbf{\Theta}^n$ denote the vector whose ijk component is $\phi(x_i, y_j, z_k, t_n)$. Inserting $\mathbf{\Theta}^n$ into the finite difference relation (14), expanding in a Taylor series, and taking into account (2), we find that

$$\mathbf{A}[\mathbf{\Theta}^{n+1} - \mathbf{\Theta}^n] + \Delta t\, \mathbf{B}[\mu \mathbf{\Theta}^{n+1} + (1-\mu)\mathbf{\Theta}^n] = \Delta t\, \mathbf{I}^n + \Delta t\, h^3 \boldsymbol{\tau}_n, \tag{19}$$

where $\boldsymbol{\tau}_n$ is the truncation error. If ϕ has three time derivatives and four space derivatives, then $\boldsymbol{\tau}_n$ satisfies an inequality of the form

$$\|\boldsymbol{\tau}_n\|_\infty \leqslant c\, \Delta t^m + ch^2,$$

where $m=1$ if $\mu \neq \frac{1}{2}$, $m=2$ if $\mu = \frac{1}{2}$, and c is a constant depending on the derivatives of ϕ. Subtracting (19) from (14) gives us the following recurrence for the error $\mathbf{\Phi} - \mathbf{\Theta}$:

$$\mathbf{\Phi}^{n+1} - \mathbf{\Theta}^{n+1} = \mathbf{C}^{-1}\mathbf{D}(\mathbf{\Phi}^n - \mathbf{\Theta}^n) + \Delta t\, h^3 \mathbf{C}^{-1} \boldsymbol{\tau}_n. \tag{20}$$

Since $h^{-3}\mathbf{C}$ is essentially a discrete approximation to the Laplacian operator, the max-norm of $[h^{-3}\mathbf{C}]^{-1} = h^3\mathbf{C}^{-1}$ is bounded by a constant independent of

h: $h^3 \|\mathbf{C}^{-1}\|_\infty \leqslant c$, where c is a constant independent of h (a brief proof of this result for Dirichlet boundary conditions appears in Appendix 2). It follows from (20) that

$$\mathbf{\Phi}^n - \mathbf{\Theta}^n = \mathbf{M}^n(\mathbf{\Phi}^0 - \mathbf{\Theta}^0) + \sum_{l=0}^{n-1} \Delta t\, \mathbf{M}^l h^3 \mathbf{C}^{-1} \boldsymbol{\tau}_{n-l-1}, \tag{21}$$

where $\mathbf{M} = \mathbf{C}^{-1}\mathbf{D}$. If σ is a constant and μ is between $\frac{1}{2}$ and 1, then

$$\|\mathbf{M}\|_\infty = \left| \frac{\varepsilon - \Delta t(1-\mu)\sigma}{\varepsilon + \Delta t\, \mu\sigma} \right| < 1.$$

Moreover, if σ is constant, μ is between 0 and $\frac{1}{2}$, and (17) holds, then $\|\mathbf{M}\|_\infty \leqslant 1$. In general, when σ varies Lipschitz continuously with position, the max-norm of $\mathbf{M}$ satisfies an inequality of the form $\|\mathbf{M}\|_\infty \leqslant 1 + c\,\Delta t$ for Δt sufficiently small where c is a constant which depends on the Lipschitz constant for σ but which is essentially independent of h (see Appendix 2). Taking the norm of (21) and making use of the inequality $\|\mathbf{M}\|_\infty \leqslant 1 + c\,\Delta t \leqslant e^{c\Delta t}$, we conclude that

$$\|\mathbf{\Phi}^n - \mathbf{\Theta}^n\|_\infty \leqslant e^{nc\Delta t} \left(\|\mathbf{\Phi}^0 - \mathbf{\Theta}^0\|_\infty + h^3 \|\mathbf{C}^{-1}\|_\infty \sum_{l=0}^{n-1} \Delta t\, \|\boldsymbol{\tau}_l\|_\infty \right).$$

If $\|\mathbf{\Phi}^0 - \mathbf{\Theta}^0\|_\infty = O(h^2)$, then it follows from the uniform bound for $h^3\mathbf{C}^{-1}$ and for the truncation error given previously, that

$$\|\mathbf{\Phi}^n - \mathbf{\Theta}^n\|_\infty = O(\Delta t^m) + O(h^2),$$

where $m = 2$ for the Crank–Nicholson scheme while $m = 1$ for $0 \leqslant \mu \leqslant 1$, $\mu \neq \frac{1}{2}$.

5. Lightning

Whenever the electric field in a region reaches the breakdown threshold E_B, the conductivity increases by many orders of magnitude. To model lightning, one can test the value of the potential gradient (or the electric field) during each time step, chop the time step whenever the electric field reaches the breakdown threshold, increase the conductivity in the breakdown region by several orders of magnitude, and continue the time step using this adjusted $\mathbf{B}$ matrix in (14). (We do not take into account the effect of heating due to lightning in our model.) In making this strategy more precise, we must specify the region where the conductivity is adjusted. Rather than monitor the magnitude of $\mathbf{E}$, it is more convenient to monitor the individual gradients $\partial_l^+ \phi_{ijk}$. When $|\partial_l^+ \phi_{ijk}|$ reaches E_B, the conductivity is increased in the region between the nodes involved in the finite difference $\partial_l^+ \phi_{ijk}$. For example, if $l = 1$ and $|\partial_l^+ \phi_{ijk}| \geqslant E_B$, then the conductivity in the region between (x_i, y_j, z_k) and (x_{i+1}, y_j, z_k) is increased by several orders of magnitude.

When the electric field reaches the breakdown threshold and the conductivity

increases, how large should we make the conductivity? It turns out that the precise value of the conductivity after breakdown really does not matter provided the conductivity is large. To see this, we utilize the Inverse Matrix Modification Formula (see [8; 7, Section 2-8; 6]) Suppose that the electric field first reaches the breakdown threshold at time level n. In the next instant of time, there is a rapid change in the potential which essentially equilibrates the potential in the breakdown region. Using a backward-difference time step to determine the adjustment in the potential due to breakdown, we have

$$(\mathbf{A} + \Delta t\, \mathbf{B} + \tau \mathbf{w}\mathbf{w}^{\mathrm{T}})\boldsymbol{\Phi}^{n+1} = \mathbf{A}\boldsymbol{\Phi}^{n} + \Delta t\, \mathbf{I}^{n},$$

where $\mathbf{w}$ is a vector with every component equal to zero for two components; one of these components is $+1$ and the other is -1. These nonzero components correspond to the nodes associated with breakdown. The parameter τ is a large number corresponding to the conductivity after breakdown. Since the potential changes rapidly during breakdown, we will let Δt tend to zero. Hence, $\boldsymbol{\Phi}^{n+1}$ is given by

$$\boldsymbol{\Phi}^{n+1} = \lim_{\tau \to \infty} (\mathbf{A} + \tau \mathbf{w}\mathbf{w}^{\mathrm{T}})^{-1}\, \mathbf{A}\boldsymbol{\Phi}^{n}.$$

By the Inverse Matrix Modification Formula, we have

$$\boldsymbol{\Phi}^{n+1} = \boldsymbol{\Phi}^{n} - \mathbf{A}^{-1}\mathbf{w}(\mathbf{w}^{\mathrm{T}}\mathbf{A}^{-1}\mathbf{w})^{-1}\mathbf{w}^{\mathrm{T}}\boldsymbol{\Phi}^{n}.$$

Thus the perturbation in the potential due to breakdown is the vector $\mathbf{A}^{-1}\mathbf{w}$ times the amplification factor $-\mathbf{w}^{\mathrm{T}}\boldsymbol{\Phi}^{n}/\mathbf{w}^{\mathrm{T}}\mathbf{A}^{-1}\mathbf{w}$. Since we let the time step Δt tend to zero, $t_{n+1} = t_n$.

After evaluating the new potential, we again examine the electric field to see if it exceeds the breakdown threshold at other points. In a typical stroke of lightning, the newly computed potential has the property that the electric field at a point adjacent to the previous breakdown point now exceeds the breakdown threshold. When there are several links in the mesh where the electric field has reached the breakdown threshold, the equation for the adjusted potential has the form

$$\boldsymbol{\Phi}^{n+1} = \lim_{\tau \to \infty} (\mathbf{A} + \tau \mathbf{W}\mathbf{W}^{\mathrm{T}})^{-1}\, \mathbf{A}\boldsymbol{\Phi}^{n},$$

where $\mathbf{W}$ is a matrix and each column of $\mathbf{W}$ is completely zero except for a $+1$ entry and a -1 entry corresponding to each pair of adjacent nodes where the electric field exceeds the breakdown threshold. Again applying the Inverse Matrix Modification Formula, we have

$$\boldsymbol{\Phi}^{n+1} = \boldsymbol{\Phi}^{n} - \mathbf{A}^{-1}\mathbf{W}(\mathbf{W}^{\mathrm{T}}\mathbf{A}^{-1}\mathbf{W})^{-1}\mathbf{W}^{\mathrm{T}}\boldsymbol{\Phi}^{n}. \tag{22}$$

We may have to apply this formula several times as the lightning propagates. Finally, when the electric field is beneath the breakdown threshold everywhere, we return to (14) and perform time steps in the usual fashion.

Typically, the electric field first reaches the breakdown threshold in the middle of some time step. To determine the first instant of breakdown, we perform the standard time step (15) and evaluate the electric field at time level n and $n+1$. Using linear interpolation, the instant of time between t_n and t_{n+1} where the electric field first exceeds the breakdown threshold can be determined. When implementing the discharge step (22), we often do not perform a full step in the sense that we move from $\mathbf{\Phi}^n$ to the $\mathbf{\Phi}^{n+1}$ given by (22). Instead, we move along the line segmenting connecting $\mathbf{\Phi}^n$ to $\mathbf{\Phi}^{n+1}$ until the electric field first exceeds the breakdown threshold at a new point. A column is appended to $\mathbf{W}$ corresponding to the new breakdown and the step (22) is attempted again. In this way $\mathbf{W}$ changes one column at a time until the lightning discharges.

6. Numerical Implementation

In the absence of lightning, the implementation of (14) is well documented in the literature. Initially, we $\mathbf{LU}$ factor the coefficient matrix $\mathbf{A} + \Delta t\, \mu \mathbf{B}$, and in each time step, we solve the factored system

$$\mathbf{LU}\mathbf{\Phi}^{n+1} = [\mathbf{A} - \Delta t(1-\mu)\mathbf{B}]\mathbf{\Phi}^n + \Delta t\, \mathbf{I}^n$$

(for example, see Section 2-7 of [7]). On the other hand, the implementation of (22) is not as easy. In this section, we develop an efficient implementation of (22).

To evaluate the right side of (22), we must compute an expression of the form

$$\mathbf{V}\mathbf{S}^{-1}\mathbf{W}^{\mathrm{T}}\mathbf{f}, \qquad \text{where} \quad \mathbf{V} = \mathbf{A}^{-1}\mathbf{W}, \quad \mathbf{S} = \mathbf{W}^{\mathrm{T}}\mathbf{V}, \qquad \text{and} \qquad \mathbf{f} = \mathbf{\Phi}^n.$$

Suppose that the matrix $\mathbf{S}$ is stored as a Cholesky factorization: $\mathbf{S} = \mathbf{L}\mathbf{L}^{\mathrm{T}}$, where $\mathbf{L}$ is a lower triangular matrix. Then the evaluation of $\mathbf{r} = \mathbf{V}\mathbf{S}^{-1}\mathbf{W}^{\mathrm{T}}\mathbf{f}$ proceeds as follows:

1. Compute the matrix-vector product $\mathbf{p} = \mathbf{W}^{\mathrm{T}}\mathbf{f}$.
2. Solve the factored system $(\mathbf{L}\mathbf{L}^{\mathrm{T}})\mathbf{q} = \mathbf{p}$.
3. Compute matrix-vector product $\mathbf{r} = \mathbf{V}\mathbf{q}$.

We must repeat this computation for several different $\mathbf{W}$ matrices where each matrix differs from the previous one by a single column. If a column is added to $\mathbf{W}$ (or deleted from $\mathbf{W}$), then a column is added to $\mathbf{V} = \mathbf{A}^{-1}\mathbf{W}$ (or deleted from $\mathbf{V}$). Hence, it is easy to update $\mathbf{V}$ following changes in $\mathbf{W}$. Now consider the impact of a change in $\mathbf{W}$ on the Cholesky factorization $\mathbf{S} = \mathbf{L}\mathbf{L}^{\mathrm{T}}$.

If the old $\mathbf{W}$ has $m-1$ columns and we add a new column to the right side of $\mathbf{W}$, then the new $\mathbf{S}$ matrix has the following structure:

$$\mathbf{S}^{\text{new}} = \begin{bmatrix} & & s_1 \\ & \mathbf{S}^{\text{old}} & \vdots \\ s_1 & \cdots & s_m \end{bmatrix},$$

where $\mathbf{s} = \mathbf{W}^{\mathrm{T}}\mathbf{v}_m$ and $\mathbf{v}_m$ is the new mth column of $\mathbf{V}$. From the structure of the new $\mathbf{S}$, it follows that the $(m-1)$th leading submatrix of the new $\mathbf{L}$ is identical to the $(m-1)$th leading submatrix of the original $\mathbf{L}$. Moreover, the elements in row m of the new $\mathbf{L}$ are

$$l_{mj} = \left(s_j - \sum_{k=1}^{j-1} l_{jk} l_{mk} \right) \Big/ l_{jj}$$

for $j = 1$ to $m-1$ and

$$l_{mm} = \sqrt{s_m - \sum_{k=1}^{m-1} l_{mk}^2}.$$

For completeness, let us also consider the deletion of a column. If column k is deleted from $\mathbf{W}$, then column k and row k are deleted from $\mathbf{S}$. The new $\mathbf{S}$ can be expressed $\mathbf{S}^{\text{new}} = \mathbf{M}\mathbf{M}^{\mathrm{T}}$, where $\mathbf{M}$ is the same as $\mathbf{L}$ but with row k deleted. The structure of $\mathbf{M}$ is indicated in Fig. 1—the top part of the matrix is zero while the bottom part is generally nonzero. The basic idea is to annihilate the "superdiagonal" elements of $\mathbf{M}$ using an orthogonal matrix $\mathbf{G}$. Since $\mathbf{G}\mathbf{G}^{\mathrm{T}} = \mathbf{I}$, we have $\mathbf{S}^{\text{new}} = \mathbf{M}\mathbf{G}(\mathbf{M}\mathbf{G})^{\mathrm{T}}$. Deleting the last column of $\mathbf{M}\mathbf{G}$, which is zero, we obtain the lower triangular Cholesky factor of the new $\mathbf{S}$.

To annihilate the superdiagonal elements of $\mathbf{M}$, we postmultiply $\mathbf{M}$ by a sequence of Givens rotations. A Givens rotation is an orthogonal matrix with the following structure:

$$\begin{bmatrix}
1 & & & & & & & \\
 & \ddots & & & & & & \\
 & & \ddots & & & & & \\
 & & & 1 & & & & \\
 & & & & c & -s & & \\
 & & & & s & c & & \\
 & & & & & & 1 & \\
 & & & & & & & \ddots \\
 & & & & & & & & 1
\end{bmatrix}$$

where $c^2 + s^2 = 1$. Observe that if

$$c = \frac{x_1}{\sqrt{x_1^2 + x_2^2}} \qquad \text{and} \qquad s = \frac{x_2}{\sqrt{x_1^2 + x_2^2}},$$

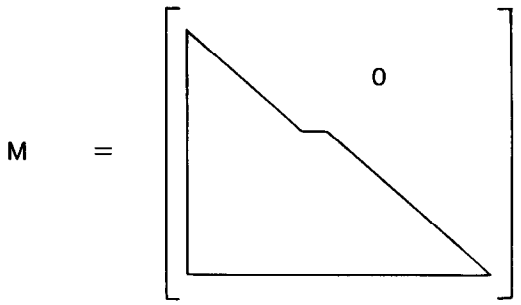

FIG. 1. The matrix **M** obtained from **L** by deleting row k.

then $c^2 + s^2 = 1$ and

$$[x_1, x_2]\begin{bmatrix} c & -s \\ s & c \end{bmatrix} = [\sqrt{x_1^2 + x_2^2}, 0].$$

In other words, the second component of **x** is annihilated and the first component is replaced by the length of **x**. Finally, **G** is the product of the Givens rotations that annihilate the nonzero superdiagonal elements depicted in Fig. 1. The lower triangular Cholesky factor of the new **S** is obtained by deleting the last column of **MG**.

In detail, if **W** has m columns and column k is deleted, then the updated Cholesky factor **L** of **S** is obtained by the following procedure:

$j = k$ to $m - 1$
  $p \leftarrow j + 1$
  if $l_{jp} = 0$ goto next j
  $t \leftarrow [l_{jp}^2 + l_{jj}^2]^{1/2}$
  $c \leftarrow l_{jj}/t$ and $s \leftarrow l_{jp}/t$
  $i = j$ to $m - 1$
    $t \leftarrow l_{ip}$
    $l_{ip} \leftarrow tc - sl_{ij}$
    $l_{ij} \leftarrow l_{ij}c + st$
  next i
next j

See Section 10 of the review article [8] for references related to updating a Cholesky factorization.

7. Numerical Experiments

In this section, we give a brief report on some numerical experiments using the scheme (14) and the treatment of lightning presented in Section 5. More extensive simulations will be reported in a separate paper. The first two problems we solve

have known solutions which provide some indication of the type of mesh that is needed to achieve around a 1% relative error in the computed solution. In these computations, the potential was evaluated in a cylinder with height and radius equal to 100 km. Dirichlet boundary conditions were employed along the bottom and the side of the cylinder while Neumann boundary conditions were employed on the top of the cylinder.

In our first experiment, we compare the electric field at the ground generated by a current impulse to the theoretical predictions of Wilson [26]. According to Wilson's model, the change in the vertical electric field at a point on the ground R meters from the location of the current impulse at height H meters is

$$\Delta E = 10^{10}(1.8H\,\Delta Q)/R^3, \tag{23}$$

where ΔQ is the charge transfer associated with the impulse. In Table I, we compare numerical values for the electric field at the ground to the theoretical predictions of Wilson using a current impulse which generates 1 C of charge at height 4.8 km. Since the potential changes rapidly near the current impulse, we employed a fine mesh near the impulse and a coarse mesh away from the impulse. In particular, for the cylindrical coordinate system described in Appendix 1, the mesh radii and altitudes in kilometers were

$$r_j = (j-1)\tau \quad \text{for} \quad 1 \leqslant j \leqslant 10 \qquad \text{and} \qquad r_j = 9.6 + \tau s^{(j-10)} \quad \text{for} \quad 11 \leqslant j \leqslant 18,$$

TABLE I

Comparison between (23) and the Vertical Electric Field of the Model

Radius (km)	Wilson's ΔE (V/m)	Model's ΔE (V/m)
0.00	781.3	780.6
1.07	726.8	721.9
2.13	596.2	586.1
3.20	450.0	441.6
4.27	326.2	321.4
5.33	233.9	231.6
6.40	168.8	167.7
7.47	123.5	122.9
8.53	92.1	91.3
9.60	69.9	68.9
11.46	45.1	44.3
12.84	33.6	32.6
15.24	21.2	20.1
19.42	10.8	10.0
26.70	4.3	3.9
39.39	1.4	1.2
61.50	0.4	0.3
100.00	0.1	0.1

where $\tau = 1.06667$ and $s = 1.74188$, and

$$z_k = k\tau \quad \text{for} \quad 0 \leqslant k \leqslant 16 \qquad \text{and} \qquad z_k = 9.6 + \tau s^{(k-16)} \quad \text{for} \quad 17 \leqslant k \leqslant 32$$

where $\tau = 0.6$ and $s = 1.36813$. The parameters τ and s are chosen so that the final mesh point in either the radial or the vertical direction is at 100 km. Since the potential corresponding to a current impulse is symmetric about the z-axis, the computed solution is independent of the angular discretization.

In the second experiment, we compared the vertical Maxwell current density at the ground produced by a step function generator and zero capacitance ($\varepsilon = 0$) with the theoretical predictions of Holzer and Saxon [12]. Nisbet [17] shows that as a consequence of Holzer and Saxon's formulas for the electric fields, the vertical Maxwell current density at a point on the ground R meters from a current generator at height H meters and with magnitude I is given by

$$J_M = \frac{(1 + 0.5\kappa R)\, HIe^{-0.5\kappa(R+H)}}{2\pi R^3} \tag{24}$$

and $\sigma(z) = 10^{-14}e^{\kappa z}$. We take $\kappa = 2 \times 10^{-4}$ and as with the previous experiment, $H = 4800$ m. In Table II we compare (24) to the Maxwell current densities obtained from the model. Again, the agreement between the model and the theoretical predictions is quite good.

TABLE II

Comparison between (24) and the Vertical Maxwell Current Density of the Model

Radius (km)	Holzer–Saxon J_M ($\times 10^{-10}$A/m^2)	Model's J_M ($\times 10^{-10}$A/m^2)
0.00	39.1450	39.2007
1.07	36.2755	36.0193
2.13	29.4219	28.8195
3.20	21.8065	21.2831
4.27	15.4195	15.1033
5.33	10.7244	10.5613
6.40	7.4674	7.3836
7.47	5.2518	5.1997
8.53	3.7447	3.6994
9.60	2.7099	2.6592
11.46	1.5963	1.5643
12.84	1.1058	1.0644
15.24	0.6095	0.5683
19.42	0.2397	0.2133
26.70	0.0583	0.0494
39.39	0.0071	0.0061
61.50	0.0003	0.0003
100.00	0.0000	0.0000

In a third experiment, we compared results produced by our model for the electric field with data obtained for a thunderstorm observed at the Kennedy Space Center on July 11, 1978. In our model, we assume that the current term of (14) is known and we compute the potential. One way to estimate the currents is to use either a convective model or a microphysical model for the thundercloud. In a convective model, the velocity field, the temperature, the pressure, the size of water drops, and in some cases, the types and sizes of ice particles are computed using the momentum equations. Convective models for a thundercloud include those of Klemp and Wilhemson [14], Miller [15], Schlesinger [19], Chen and Orville [2], Clark [4], and Tripoli and Cotton [21, 22]. In microphysical cloud electrification models, the position of precipitation particles with respect to the airflow, temperature, and water substance fields is computed. Microphysical models for a thundercloud include those of Ziv and Levin [27], Illingworth and Latham [13], Chiu [3], Spangler and Rosenkilde [20], Wagner and Telford [25], and Tzur and Levin [23]. Models such as those of Helsdon [9] and Helsdon and Farley [10, 11] also incorporate convective dynamic effects.

Another way to estimate the currents is through experimental measurements, using field mill data to estimate the location and magnitude of current generators. This is the approach that we followed in our simulation of the storm at the Kennedy Space Center. During the storm, the electric field was measured at 25 locations on the ground within the Space Center. Using the data collected at these field mills, the vertical Maxwell current densities as well as the locations and

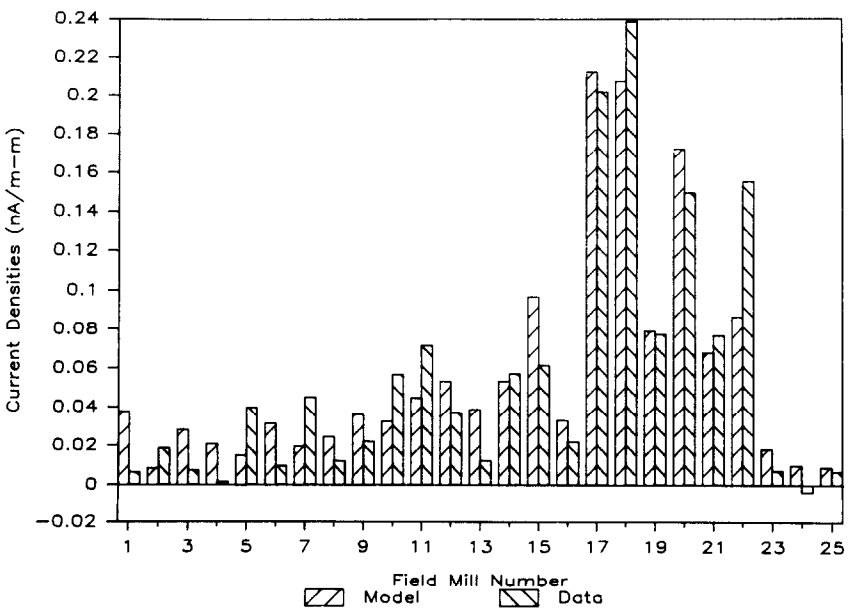

FIG. 2. Maxwell current densities for TRIP storm at 19:12 h.

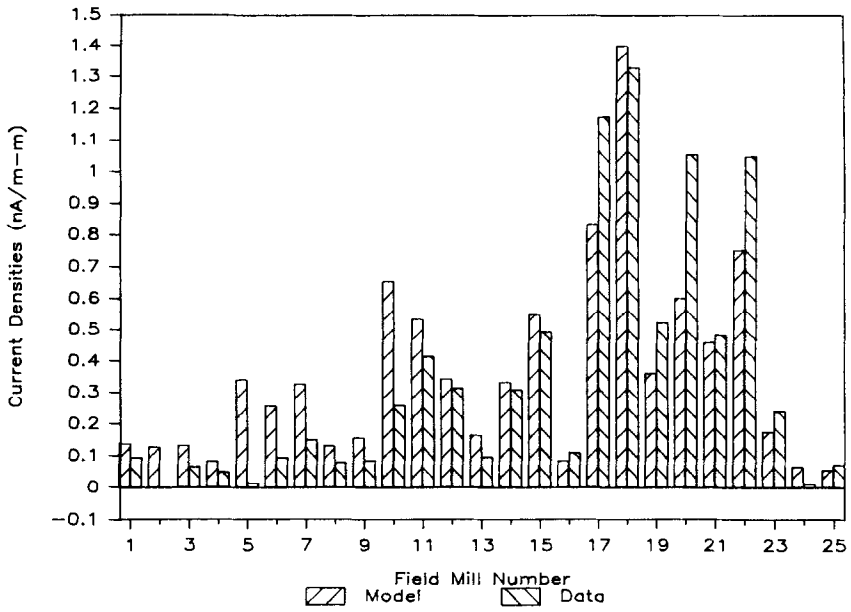

FIG. 3. Maxwell current densities for TRIP storm at 19:27 h.

magnitudes of current generators within the thundercloud were estimated (see [18]). After obtaining the current generators for the period of time to be modeled, the cloud boundaries were defined. These boundaries enclose a volume with a relatively low value for the conductivity. Using our model, we followed the development of the storm, computing the Maxwell current densities and electric field values at ground node locations for selected times. This work has proceeded to the point that the first 10 min following the initial electrification has been modeled. In Figs. 2 and 3, the Maxwell current densities from the model are compared to those of the actual storm at field mill locations. It is apparent from the figures that the model has produced results in agreement with the real storm for early storm times.

8. CONCLUSIONS

Realistic electrical models for a thunderstorm involve special problems related to the time and distance scales. The current densities flow outside the cloud to the ionosphere above and to the ground below so that the model must encompass around 100 km. Dynamic structure affecting the charged hydrometeors exists on a length scale of a kilometer while lightning channels have diameters of less than a meter. The lifetime of a thunderstorm cell is about an hour while time scales associated with electrical breakdown are less than a microsecond. In this paper, we started with Maxwell's equations and we obtained an equation governing the evolu-

tion of the electric potential under the assumption that the time derivative of the magnetic field strength can be neglected. Integrating this equation over boxes and approximating derivatives by finite differences, we generated an implicit system of difference equations governing the evolution of the electric field. Max-norm estimates were obtained for the error in the discrete potential. When the electric field reached the breakdown threshold, the electric potential changed instantaneously throughout the thrundercloud. This change was evaluated using the Inverse Matrix Modification Formula. Preliminary results for an actual storm simulation appear in Section 7.

The work in this paper is connected with convective and microphysical thunderstorm models. In these models, the motion of charged particles can be monitored and the electric field can be calculated by solving the Poisson equation

$$\varepsilon \nabla^2 \phi = \rho,$$

which is obtained from Gauss's law "$\varepsilon \nabla \cdot \mathbf{E} = \rho$" after the substitution $\mathbf{E} = \nabla \phi$. Lightning discharges are not incorporated in these models. In contrast, our model is based on Eq. (1) (Ampère's law) and lightning discharges are included in the model. Since the input to our model is the electric current associated with the motion of charged particles in the cloud, a convective or microphysical model for the charged particles in a thundercloud provides the date needed by our model to evaluate the electric field. Hence, one way to completely simulate a thunderstorm is to link together a microphysical cloud model with our model for the electric fields.

When simulating a thundercloud using the model proposed in this paper, mesh points can be 100 m apart. Obviously, with a 100 m mesh, it is not possible to get a detailed picture of a lightning stroke. However, the electric fields generated by our model combined with Gauss's law give an estimate for the charge transfer associated with a lightning stroke.

APPENDIX 1: CYLINDRICAL COORDINATES

In a cylindrical coordinate system, the unknowns are the value of the potential at a sequence of nodes positioned on rings around the z-axis. Let z_1 through z_N denote the height of the various rings, let r_1 through r_M denote the ring radii, and let θ_1 through θ_L denote the angles corresponding to nodes in a ring. Hence, the (θ, r, z) coordinates of the nodes have the form (θ_i, r_j, z_k). The cylinder is partitioned into the wedge shaped volume elements corresponding to those points (θ, r, z) which satisfy the inequalities

$$h_i \leqslant \theta \leqslant h_{i+1}, \qquad \rho_j \leqslant r \leqslant \rho_{j+1}, \quad \zeta_k \leqslant z \leqslant \zeta_{k+1}, \tag{25}$$

where h_i lies between θ_{i-1} and θ_i, ρ_j lies between r_{j-1} and r_j, and ζ_k lies between z_{k-1} and z_k. Preferably, we have

$$h_i = \frac{\theta_i + \theta_{i-1}}{2}, \qquad \rho_j = \frac{r_j + r_{j-1}}{2}, \qquad \zeta_k = \frac{z_k + z_{k-1}}{2}.$$

Letting S_{ijk} denote the surface of the volume element given by (25), observe that S_{ijk} contains the node (θ_i, r_j, z_k). Moreover, the analogue of (9) is

$$\int_{\partial S_{ijk}} \nabla\phi \cdot \mathbf{dS} \approx \left(\sum_{l=1}^{3} C_l \partial_l^+ - \sum_{l=1}^{3} D_l \partial_l^- \right) \phi_{ijk},$$

where

$$C_1 = D_1 = \frac{(\rho_{j+1} - \rho_j)(\zeta_{k+1} - \zeta_k)}{r_j},$$

$$C_2 = \rho_{j+1}(h_{i+1} - h_i)(\zeta_{k+1} - \zeta_k), \qquad D_2 = \rho_j(h_{i+1} - h_i)(\zeta_{k+1} - \zeta_k),$$

$$C_3 = D_3 = \frac{(h_{i+1} - h_i)(\rho_{j+1}^2 - \rho_j^2)}{2}.$$

The conductance integral in (8) is similar although we must take into account the variation in the conductivity with altitude. Using the average conductivity σ_k defined by (12), we have

$$\int_{\partial S_{ijk}} \sigma \nabla\phi \cdot \mathbf{dS} \approx \left(\sum_{l=1}^{2} \sigma_k (C_l \partial_l^+ - D_l \partial_l^-) + \sigma(\zeta_{k+1}) C_3 \partial_3^+ - \sigma(\zeta_k) D_3 \partial_3^- \right) \phi_{ijk}.$$

APPENDIX 2: MAX-NORM BOUNDS

In this Appendix, we establish some properties for the discrete elliptic operators that appear in Section 4. These operators arise from the discretization of the equation $-\nabla \cdot \sigma \nabla\phi = f$. Abstractly, these discretization have the form

$$-h^{-1} \sum_{l=1}^{3} [C_{ijkl} \partial_l^+ - D_{ijkl} \partial_l^-] \phi_{ijk} = f_{ijk}, \tag{26}$$

where C_{ijkl} is the value of σ at some point in the domain of interest and C_{ijkl} is related to D_{ijkl}. For example, in the case $l = 1$, $C_{ijk1} = D_{i+1,jk1}$. Letting γ denote the minimum of the C_{ijkl}, we assume that γ is positive and that C_{ijkl} is independent of either i or j or k. To be specific, suppose that C_{ijkl} is independent of i. Let N^h denote the set of indices i, j, and k for which (26) should hold. It is assumed that N^h is a bounded set in the first octant. We consider Dirichlet boundary conditions so that ϕ_{ijk} is constrained to be zero whenever (i, j, k) is outside N^h. Let Φ denote the

vector containing the ϕ_{ijk} for (i, j, k) in N^h and let $\mathbf{A}$ denote the coefficient matrix corresponding to (26). $\mathbf{A}$ is symmetric provided the Eqs. (26) are written down in the same order that the ϕ_{ijk} are inserted into the array $\mathbf{\Phi}$. If $I-1$ is the maximum value of the index i associated with points in the set N^h and if a denotes the product hI, we will show that

$$\|\mathbf{A}^{-1}\|_\infty \leqslant a^2/\gamma. \tag{27}$$

By Corollary 1 on page 85 of [24], the elements of $\mathbf{A}^{-1}$ are nonnegative. Hence, $\|\mathbf{A}^{-1}\|_\infty = \|\mathbf{A}^{-1}\mathbf{1}\|_\infty$, where $\mathbf{1}$ is the vector with every component equal to 1. Furthermore, $\|\mathbf{A}^{-1}\|_\infty \leqslant \|\mathbf{A}^{-1}\mathbf{F}\|_\infty$ if $\mathbf{F} \geqslant \mathbf{1}$. Defining $\psi_{ijk} = -(hi)^2/2\gamma$, observe that $\partial_2\psi_{ijk} = \partial_3\psi_{ijk} = 0$, since ψ_{ijk} is independent of j and k. Letting C_{jk} denote C_{ijk1} (recall that C_{ijk1} is independent of i) and evaluating the left side of (26) for $\phi_{ijk} = \psi_{ijk}$ yields

$$\frac{C_{jk}}{2\gamma}\left[\frac{h^2[(i+1)^2 - i^2]}{h^2} - \frac{h^2[i^2 - (i-1)^2]}{h^2}\right] \geqslant 1. \tag{28}$$

Define $\lambda_{ijk} = (hi)^2/2\gamma$ for (i, j, k) outside N^h while for $(i, j, k) \in N^h$, choose λ_{ijk} so that it satisfies the equation

$$\sum_{l=1}^{3} [C_{ijkl}\partial_l^+ - D_{ijkl}\partial_l^-]\lambda_{ijk} = 0. \tag{29}$$

By the maximum principle, $|\lambda_{ijk}|$ for (i, j, k) in N^h is bounded by the magnitude of $|\lambda_{ijk}|$ for (i, j, k) just outside N^h. Hence, for (i, j, k) in N^h, $|\lambda_{ijk}| \leqslant a^2/2\gamma$. If ϕ_{ijk} is the sum $\psi_{ijk} + \lambda_{ijk}$, then ϕ_{ijk} vanishes for (i, j, k) outside N^h while

$$-h^{-1}\sum_{l=1}^{3}\left[C_{ijkl}\partial_l^+ - D_{ijkl}\partial_l^-\right]\phi_{ijk} \geqslant 1$$

for (i, j, k) in N^h. Again, letting $\mathbf{\Phi}$, $\mathbf{\Psi}$, and $\mathbf{\Lambda}$ denote the vectors formed from ϕ_{ijk}, ψ_{ijk}, and λ_{ijk} for (i, j, k) in N^h, we have

$$\|\mathbf{A}^{-1}\|_\infty \leqslant \|\mathbf{\Phi}\|_\infty = \|\mathbf{\Psi} + \mathbf{\Lambda}\|_\infty \leqslant \|\mathbf{\Psi}\|_\infty + \|\mathbf{\Lambda}\|_\infty \leqslant \frac{a^2}{2\gamma} + \frac{a^2}{2\gamma} = \frac{a^2}{\gamma}.$$

This establishes (27).

The preceding analysis yields a bound for the max-norm of the inverse of the matrix $\mathbf{C}$ introduced in Section 4. Now let us consider the product $\mathbf{C}^{-1}\mathbf{D}$. From the definition of $\mathbf{C}$ and $\mathbf{D}$, we have

$$\begin{aligned}\mathbf{C}^{-1}\mathbf{D} &= (\mathbf{A} + \Delta t\,\mu\mathbf{B})^{-1}[\mathbf{A} - \Delta t(1-\mu)\,\mathbf{B}] = \mathbf{I} - \Delta t(\mathbf{A} + \Delta t\,\mu\mathbf{B})^{-1}\mathbf{B} \\ &= \mathbf{I} - \Delta t(\mathbf{I} + \Delta t\,\mu\mathbf{A}^{-1}\mathbf{B})^{-1}\mathbf{A}^{-1}\mathbf{B}.\end{aligned}$$

Taking norms gives

$$\|\mathbf{C}^{-1}\mathbf{D}\|_\infty \leqslant 1 + \frac{\Delta t \, \|\mathbf{A}^{-1}\mathbf{B}\|_\infty}{1 - \Delta t \, \mu \, \|\mathbf{A}^{-1}\mathbf{B}\|_\infty} \tag{30}$$

whenever $\Delta t \, \mu \, \|\mathbf{A}^{-1}\mathbf{B}\|_\infty < 1$. We will obtain a bound for $\|\mathbf{A}^{-1}\mathbf{B}\|_\infty$ under the assumption that σ is Lipschitz continuous. In one space dimension, this bound is independent of h. In more than one space dimension, our method of analysis indicates that this bound is "essentially" independent of h. Consequently, (30) implies that for Δt sufficiently small, $\|\mathbf{C}^{-1}\mathbf{D}\|_\infty$ is bounded by an expression of the form $1 + c\,\Delta t$ where c is essentially independent of h.

First, let us consider one space dimension. In this case, $\mathbf{A}$ is ε times the symmetric tridiagonal matrix with each diagonal element equal to 2 and with each superdiagonal and subdiagonal element equal to -1. For convenience assume that $\varepsilon = 1$. Similarly, $\mathbf{B}$ is the symmetric tridiagonal matrix defined by

$$b_{i,i+1} = -\sigma_i \qquad \text{and} \qquad b_{ii} = \sigma_i + \sigma_{i-1},$$

where σ_i is the value of σ at $x = (i + 0.5)h$. (Actually, $\mathbf{A}$ and $\mathbf{B}$ are multiplied by powers of h, but when $\mathbf{A}^{-1}\mathbf{B}$ is computed, these powers of h cancel.) The nonzero elements in the kth column of $\mathbf{B}$ have the form

$$\begin{bmatrix} -\sigma_{k-1} \\ \sigma_k + \sigma_{k-1} \\ -\sigma_k \end{bmatrix},$$

which can be rewritten

$$\sigma_k \begin{bmatrix} -1 \\ 2 \\ -1 \end{bmatrix} + (\sigma_k - \sigma_{k-1}) \begin{bmatrix} 1 \\ -1 \\ 0 \end{bmatrix}. \tag{31}$$

Letting $\boldsymbol{\delta}^k$ denote the vector with every component equal to zero except for component k which is one, $\mathbf{A}^{-1}$ times the vector corresponding to the first term in (31) is $\sigma_k \boldsymbol{\delta}^k$. Now consider the product between $\mathbf{A}^{-1}$ and the vector corresponding to the second term in (31). This product can be expressed $(\sigma_k - \sigma_{k-1})\,\mathbf{A}^{-1}(\boldsymbol{\delta}^{k-1} - \boldsymbol{\delta}^k)$. By the Lipschitz continuity of σ,

$$|\sigma_k - \sigma_{k-1}| \leqslant ch$$

where c is the Lipschitz constant.

The vector $\boldsymbol{\Phi} = \mathbf{A}^{-1}(\boldsymbol{\delta}^{k-1} - \boldsymbol{\delta}^k)$ can be constructed in the following way: Let $\boldsymbol{\Psi}$ be the vector given by

$$\psi_i = 0 \quad \text{for} \quad i \geqslant k \qquad \text{and} \qquad \psi_i = 1 \quad \text{for} \quad i < k.$$

It is easily verified that

$$-\psi_{i-1}+2\psi_i-\psi_{i+1}=\begin{cases}0 & \text{for } i>k \text{ or } i<k-1,\\ -1 & \text{for } i=k,\\ 1 & \text{for } i=k-1.\end{cases}$$

Suppose that $\mathbf{A}$ is $I\times I$ and let Λ be chosen so that

$$\lambda_0=-1, \qquad \lambda_{I+1}=0, \qquad -\lambda_{i-1}+2\lambda_i-\lambda_{k+1}=0 \qquad \text{for } 1\leqslant i\leqslant I.$$

By the maximum principle, $\|\Lambda\|_\infty\leqslant 1$, and by construction, $\|\Psi\|_\infty=1$ while $\mathbf{A}(\Psi+\Lambda)=\delta^{k-1}-\delta^k$. Thus $\Psi+\Lambda=\mathbf{A}^{-1}(\delta^{k-1}-\delta^k)$. Since the max-norm of both Ψ and Λ are bounded by 1, the max-norm of $\mathbf{A}^{-1}(\delta^{-1}-\delta^k)$ is bounded by 2. Moreover, each element of the vector $(\sigma_k-\sigma_{k-1})\mathbf{A}^{-1}(\delta^{k-1}-\delta^k)$ is bounded by $2ch$, where c is the Lipschitz constant for σ. Collecting these observations, we see that $\mathbf{A}^{-1}\mathbf{B}$ is the sum of a diagonal matrix with the σ_k on the diagonal and another matrix with each element bounded by $2ch$. Letting a denote the product hI, it follows that in one dimension,

$$\|\mathbf{A}^{-1}\mathbf{B}\|_\infty\leqslant \text{maximum } \sigma+2a \text{ maximum } \left|\frac{d\sigma}{dx}\right|.$$

(Recall that the Lipschitz constant for a function is bounded by its maximum derivative.) If $\varepsilon\neq 1$, then the right side of this inequality is divided by ε.

Now consider two space dimensions and a rectangular domain. Let $\mathbf{T}$ denote the symmetric tridiagonal matrix with 2's on the diagonal and with -1's on the superdiagonal and on the subdiagonal. Then $\mathbf{A}$ is the sum of a block diagonal matrix with $\mathbf{T}$'s on the diagonal and a symmetric block tridiagonal matrix with $2\mathbf{I}$ for each diagonal element and with $-\mathbf{I}$ on the superdiagonal and on the subdiagonal. Similarly, $\mathbf{B}$ is the sum $\mathbf{D}+\mathbf{C}$ of a block diagonal matrix $\mathbf{D}$ and a symmetric block tridiagonal matrix $\mathbf{C}$, however, since σ varies with position, the diagonal blocks $\mathbf{T}_1, \mathbf{T}_2, \ldots, \mathbf{T}_m$ of $\mathbf{D}$ are not all the same. Likewise, the diagonal blocks as well as the off-diagonal blocks of $\mathbf{C}$ may depend on their location in the matrix. Factoring $\mathbf{T}$ from each row of the block matrix $\mathbf{A}$, the product $\mathbf{A}^{-1}\mathbf{D}$ can be expressed in the following form:

$$\mathbf{A}^{-1}\mathbf{D}=\begin{bmatrix}\mathbf{I}+2\mathbf{T}^{-1} & -\mathbf{T}^{-1} & & & \\ -\mathbf{T}^{-1} & \mathbf{I}+2\mathbf{T}^{-1} & & & \\ & & \ddots & & \\ & & & & -\mathbf{T}^{-1} \\ & & & -\mathbf{T}^{-1} & \mathbf{I}+2\mathbf{T}^{-1}\end{bmatrix}^{-1}$$

$$\times\begin{bmatrix}\mathbf{T}^{-1}\mathbf{T}_1 & & & \\ & \mathbf{T}^{-1}\mathbf{T}_2 & & \\ & & \ddots & \\ & & & \mathbf{T}^{-1}\mathbf{T}_m\end{bmatrix}. \tag{32}$$

By the 1-dimensional analysis given previously, the max-norm of each product $\mathbf{T}^{-1}\mathbf{T}_k$ is bounded by a constant that is independent of h. Let $\mathbf{E}$ denote the first factor on the right side of (32). Even though $\mathbf{E}$ is difficult to analyze using the max-norm, this matrix is independent of σ—it just depends on the size of the mesh. Hence, $\mathbf{E}$ can be evaluated on a computer and a numerical value for $\|\mathbf{E}\|_\infty$ can be obtained. If $\mathbf{T}$ is 10×10 and $m = 10$, so that $\mathbf{E}$ is 100×100, then $\|\mathbf{E}\|_\infty \approx 1.67$. If $\mathbf{T}$ is 20×20 and $m = 20$, so that $\mathbf{E}$ is 400×400, then $\|\mathbf{E}\|_\infty \approx 2.08$. If $\mathbf{T}$ is 40×40 and $m = 40$, so that $\mathbf{E}$ is 1600×1600, then $\|\mathbf{E}\|_\infty \approx 2.50$. It appears that $\|\mathbf{E}\|_\infty$ is proportional to the logarithm of the matrix dimension. In summary, for two space dimensions, we have the bound

$$\|\mathbf{A}^{-1}\mathbf{D}\|_\infty \leqslant 2.5 \left\{ \text{maximum } \sigma + 2a \text{ maximum } \left| \frac{d\sigma}{dx} \right| \right\}, \tag{33}$$

which applies to matrices with up to a million elements.

Now consider the product $\mathbf{A}^{-1}\mathbf{C}$. Note that pivoting two columns or two rows does not change the max-norm of a matrix. Also, by reordering the unknowns (or equivalently, by applying a sequence of row and column interchanges to $\mathbf{C}$ and $\mathbf{A}$), $\mathbf{C}$ can be transformed to a block diagonal matrix like $\mathbf{D}$. Since these pivots leave $\mathbf{A}$ invariant, it follows that the estimate (33) also applies to the product $\mathbf{A}^{-1}\mathbf{C}$. In conclusion, for two space dimension and for matrices with up to a million elements, we have

$$\|\mathbf{A}^{-1}\mathbf{B}\|_\infty \leqslant 2.5 \left\{ 2 \max \sigma + 2a \max \left| \frac{d\sigma}{dx} \right| + 2b \max \left| \frac{d\sigma}{dy} \right| \right\},$$

where b denotes the maximum product jh corresponding to points (i, j) in the domain.

Three dimensions can be analyzed in the same fashion—the matrix $\mathbf{A}$ is written as the sum of three matrices. One of these matrices is block diagonal with $\mathbf{T}$'s on the diagonal. We factor $\mathbf{T}$ from each row of the block matrix $\mathbf{A}$ and we proceed as we did previously. Terms of the form $\|\mathbf{T}^{-1}\mathbf{T}_k\|_\infty$ are bounded by the 1-dimensional analysis while the max-norm of the 3-dimensional analogue to $\mathbf{E}$ can be evaluated on a computer. For example, if $\mathbf{T}$ is 5×5, so that $\mathbf{E}$ is 125×125, then $\|\mathbf{E}\|_\infty \approx 1.30$. If $\mathbf{T}$ is 10×10, so that $\mathbf{E}$ is 1000×1000, then $\|\mathbf{E}\|_\infty \approx 1.78$. In conclusion, for three space dimensions and for matrices with up to a million elements, we have

$$\|\mathbf{A}^{-1}\mathbf{B}\|_\infty \leqslant 1.78 \left\{ 3 \max \sigma + 2a \max \left| \frac{d\sigma}{dx} \right| + 2b \max \left| \frac{d\sigma}{dy} \right| + 2c \max \left| \frac{d\sigma}{dz} \right| \right\},$$

where c denotes the maximum product kh corresponding to points (i, j, k) in the domain.

REFERENCES

1. G. L. BROWNING, I. TZUR, AND R. G. ROBLE, *J. Atmos. Sci.* **44**, 2166 (1987).
2. C.-H. CHEN AND H. D. ORVILLE, *J. Appl. Meteorol.* **19**, 256 (1980).
3. C.-S. CHIU, *J. Geophys. Res.* **83**, 5025 (1978).
4. T. L. CLARK, *J. Atmos. Sci.* **36**, 2191 (1979).
5. G. S. FORBES, J. S. NISBET, AND T. BARNARD, *EOS Trans.* **66**, 835 (1985).
6. W. W. HAGER, *J. Optim. Theory Appl.* **55**, 37 (1987).
7. W. W. HAGER, *Applied Numerical Linear Algebra* (Prentice–Hall, Englewood Cliffs, NJ, 1988).
8. W. W. HAGER, Updating the inverse of a matrix, *SIAM Rev.* **31**, 221 (1989).
9. J. H. HELSDON, JR., *J. Appl. Meteorol.* **19**, 1101 (1980).
10. J. H. HELSDON, JR. AND R. D. FARLEY, *J. Geophys. Res.* **92**, 5645 (1987).
11. J. H. HELSDON, JR. AND R. D. FARLEY, *J. Geophys. Res.* **92**, 5661 (1987).
12. R. E. HOLZER AND D. S. SAXON, *J. Geophys. Res.* **57**, 207 (1952).
13. A. J. ILLINGWORTH AND J. LATHAM, *Q. J. Roy. Meteorol. Soc.* **103**, 281 (1977).
14. J. B. KLEMP AND R. B. WILHELMSON, *J. Atmos. Sci.* **35**, 1070 (1978).
15. M. J. MILLER, *Q. J. Roy. Meteorol. Soc.* **104**, 413 (1978).
16. J. S. NISBET, *J. Atmos. Sci.* **40**, 2855 (1983).
17. J. S. NISBET, *J. Geophys. Res.* **90**, 5840 (1985).
18. J. S. NISBET, T. A. BARNARD, G. S. FORBES, E. P. KRIDER, R. LHERMITTE, AND C. L. LENNON, A case study of the TRIP thunderstorm of July 11, 1978. I. Analysis of the data base, Pennsylvania State University Communications and Space Sciences Laboratory, Report PSU-CSSL-PA-87/12, 1987.
19. R. E. SCHLESINGER, *J. Atmos. Sci.* **35**, 690 (1978).
20. J. D. SPANGLER AND C. E. ROSENKILDE, *J. Geophys. Res.* **84**, 3184 (1979).
21. G. L. TRIPOLI AND W. R. COTTON, *J. Appl. Meteorol.* **19**, 1037 (1980).
22. G. L. TRIPOLI AND W. R. COTTON, *J. Rech. Atmos.* **16**, 185 (1982).
23. I. TZUR AND Z. LEVIN, *J. Atmos. Sci.* **38**, 2444 (1981).
24. R. S. VARGA, *Matrix Iterative Analysis*, (Prentice–Hall, Englewood Cliffs, NJ, 1962).
25. P. B. WAGNER AND J. W. TELFORD, *J. Rech. Atmos.* **15**, 97 (1981).
26. C. T. R. WILSON III, *Philos. Trans. Roy. Soc. London A* **115**, 73 (1920).
27. A. ZIV AND Z. LEVIN, *J. Atmos. Sci.* **31**, 1652 (1974).